Received: 26 February 2024 | Accepted: 27 June 2024 | Published online: 14 August 2024

DOI: 10.1002/agj2.21654

Agronomy Journal

ORIGINAL ARTICLE

Biometry, Modeling, and Statistics

Simulating the development and growth of lentil using the CSM-CROPGRO model

Qi Jing[1] | Kenneth J. Boote[2] | Kui Liu[3] | Gerrit Hoogenboom[2] | Jeffrey W. White[2] | Ward Smith[1] | Guillaume Jégo[4] | Brian Grant[1] | Marianne Crépeau[4] | Jiali Shang[1] | Jiangui Liu[1] | Aston Chipanshi[5] | Budong Qian[1]

[1]Science and Technology Branch, Agriculture and Agri-Food Canada, Ottawa, Ontario, Canada

[2]Department of Agricultural and Biological Engineering, University of Florida, Gainesville, Florida, USA

[3]Science and Technology Branch, Agriculture and Agri-Food Canada, Swift Current, Saskatchewan, Canada

[4]Science and Technology Branch, Agriculture and Agri-Food Canada, Quebec City, Quebec, Canada

[5]Science and Technology Branch, Agriculture and Agri-Food Canada, Regina, Saskatchewan, Canada

Correspondence
Qi Jing and Budong Qian, Science and Technology Branch, Agriculture and Agri-Food Canada, Ottawa, ON K1A 0C6, Canada.
Email: qi.jing@agr.gc.ca and budong.qian@agr.gc.ca

Assigned to Associate Editor Stephen Del Grosso.

Funding information
Agriculture and Agri-Food Canada, Grant/Award Numbers: J-002303, J-003082

Abstract

The pulse crop lentil (*Lens culinaris* Medik.) is often grown in crop rotations to provide nitrogen (N) and water benefits for subsequent crops. Lentil yields vary greatly with environmental factors and management. A reliable crop model for lentil could assist efforts to assess the effects of management practices to mitigate environmental stresses and maximize lentil yields. However, few crop models simulate the development and growth of lentil. In this study, we adapted the CSM-CROPGRO model in the Decision Support System for Agrotechnology Transfer to simulate lentil development and growth based on data collected from six experiments conducted from 2001 to 2021 globally. The initial parameter values taken from faba bean (*Vicia faba* L.) were modified based on reported information and analysis of observed data. Those values were fine-tuned to minimize the gaps between the simulated and observed crop attributes. The model simulated well development stages with root mean square error (RMSE) of 4 days and aboveground biomass with normalized root mean square error (nRMSE ≤ 23%). Seed yields were generally well simulated across experiments in calibration and validation (nRMSE = 19%) datasets, except for overestimation under the humid environment of Quebec in Canada, which may have resulted from excessive vegetative growth. The underlying mechanisms leading to excessive vegetative growth need to be explored further and included in the model for evaluating the adaptability of lentils to specific regions. Overall, the CSM-CROPGRO-Lentil model is ready for simulating lentil production under various scenarios, which may identify ways to improve the productivity and resiliency of cropping systems that include lentil.

Abbreviations: AGB, aboveground dry biomass; DSSAT, Decision Support System for Agrotechnology Transfer; EF, model simulation efficiency; LAI, leaf area index; ME, mean error; nRMSE, normalized RMSE; rME, relative ME; RMSE, the root mean square error; SLA, specific leaf area.

1 | INTRODUCTION

Lentil is one of the most important pulse crops globally and is primarily grown for its protein-rich seeds used as food and feed, and industrial products. The harvested area of lentils was about 5.6 million ha globally in 2022, with 30.8% in Canada, 25.4% in India, 10.3% in Australia, 6.2% in Turkey, 4.4% in the United States, 3.9% in Russia, 3.6% in Nepal, and the remaining 15.4% in 30 other countries (FAOSTAT, 2024). Lentil is an annual crop known for its lens-shaped seeds, which include various shades of red, green, and brown, with sizes ranging from 25 g to over 60 g per 1000 seeds (Barker, 2023). Cultivated lentils are grouped into two classes, microsperma with 1000-seed weight <40 g and macrosperma above 40 g (Chahota et al., 2019). The lentil plant is highly branched, typically 30- to 50-cm tall. The leaves are pinnate, consisting of five to eight small leaflets.

Lentil is frequently chosen as an important component for diversifying cropping systems and increasing profitability on the semiarid Canadian Prairies (Gan et al., 2017). For instance, lentil uses less water than wheat, leaving deep soil profile water behind for the subsequent crops because of their shallower rooting depths (L. Liu et al., 2011). Lentil is able to derive a large proportion of its nitrogen (N) from biological N_2 fixation, which can contribute a significant net N gain to the soil after harvest (Van Kessel, 1994). Lentil in cropping rotations provides soil N benefits, which appear mainly in the top 30 cm soil layer, and significantly increase the yield of the following wheat and total protein-based production at the cropping system level (K. Liu et al., 2020). Due to many uses of lentil as food and feed, and its ability to undertake symbiotic nitrogen fixation, which is an advantage over cereal crops, lentil could be a major crop in other parts of the world. A preliminary study identified the potential to expand lentil production beyond the regions where lentil is currently grown in Africa (Ghanem et al., 2015).

Lentil is grown in diverse environments. In Canada, lentil is sown in spring and grows in progressively warming environments under extended daylength. In Mediterranean and South Asian environments, lentil is generally planted in winter and emerges under cool temperatures and short days, with significant warming and lengthening days after the spring equinox. Observations of lentil development in those diverse regions show varied responses of phenology to temperature and photoperiod (Wright et al., 2021). Lentil has a long-day photoperiod response, and some cultivars respond to vernalization (Roberts et al., 1988; Summerfield et al., 1985).

Environmental factors also play a large role in yield formation and harvest index (HI) of individual genotypes. Harvested lentil yield is about 1.2 Mg ha^{-1} on a global average with a range from 0.2 to 4.6 Mg ha^{-1} in 2022 (FAOSTAT, 2024), and the average yield in Canada is 1.34 and 0.9 Mg ha^{-1} in India. The large gap between the average and the highest yields indicates the potential for improving lentil productivity, which requires appropriate management under favorable environments using adapted cultivars. Low yields are often associated with low HI, which may vary from 0.07 to 0.56 (Whitehead et al., 2000). Conditions that cause excessive vegetative growth, particularly late-season growth, can dramatically lower the HI of lentil (Hanlan et al., 2006). Rising temperatures and drought stress are expected to limit the growth and production potential of lentil, because they markedly impair photosynthesis and carbohydrate metabolism in leaves and seeds, resulting in stunted plants with fewer and smaller seeds (Sehgal et al., 2017). Quantitative information on the developmental and physiological responses to environment for lentil may help us to design management practices to mitigate heat and drought stresses and to maximize lentil yields. Crop growth models are important tools for explicitly simulating the interactions among environmental factors, crop processes, and management practices. Their use and application can increase insight into relevant processes, allowing the study of the impact from various crop management practices and the exploration of possible consequences of management modifications and climate change.

Few crop models have been developed or adapted for lentil, although lentil has an important role in cropping systems for sustainable and resilient food production under climate change. In the 1980s, a number of studies examined and quantified the response of lentil cultivars to environmental factors (Summerfield & Muehlbauer, 1981; Summerfield et al., 1984, 1985, 1989a, 1989b). Their findings under field and controlled environments added quantitative information on the impacts of environmental factors on lentil development and growth, especially for the temperature and photoperiod on lentil development. Such quantitative information is useful for adapting the CSM-CROPGRO model in Decision Support System for Agrotechnology Transfer (DSSAT) (Hoogenboom et al., 2019, 2023) to model lentil development and growth. The CSM-CROPGRO model was originally developed to simulate soybean [*Glycine max* (L.) Merr.] development and growth accounting for the cultivar interactions with environment and management, considering the characteristics of

Core Ideas

- A reliable lentil model is required to assist in improving lentil yields under current and future climates.
- The CSM-CROPGRO model was successfully adapted to simulate lentil development and growth.
- The CROPGRO-Lentil model simulated well development stages and reproduced aboveground biomass and seed yield.

TABLE 1 Summary of field experiments across sites and years, including treatments, cultivar names, recorded development stages, and the number of measured crop attributes.

Experiment	Site	Year	Cultivar	Treatment	Recorded stages	LAI	AGB	Yield	Tissue biomass
I	Luskville, CA	2021	Maxim Impulse	–	V0, R1, R3, R5, R7	8	8	2	Leaf, stem, pod
II	Swift Current, CA	2021	Maxim Lima Impulse	Three seeding dates	V0, R1, R7	21	18	7	–
III	Brooks, CA	2011–2019	Maxim	–	R1, R7	–	7	7	–
IV	Swift Current, CA	2006–2007	Glamis	Rainfed; irrigated	R1, R7	–	15	4	Root
V	Swift Current; Stewart Valley, CA	2000–2001	Glamis	Fertilizer rates	R1, R7	–	–	10	–
VI	Nine Sites across eight countries	2016–2018	Maxim Glamis	–	V0, R1, R5, R7	–	–	–	–
VII	Saskatoon; Outlook, CA	2002	Multiple cultivars	Three population densities	–	–	6	6	–
VIII	Bozeman; Havre	2019–2021	Maxim	–	–	–	–	4	–
IX	Meknes, MA	2021–2022	Medik	Four weed control	–	–	–	2	–

Abbreviations: AGB, aboveground dry biomass; LAI, leaf area index.

legumes such as C_3 photosynthesis and symbiotic N_2 fixation (Boote et al., 1998; Hoogenboom et al., 1992). This generic model has since been adapted to simulate a number of crops, including other legumes and nonlegumes (Boote et al., 2021).

The objective of this study was to adapt the CSM-CROPGRO model in DSSAT for lentil based on experimental data collected from field experiments and literature. Field experiments from latitude 23˚N to 53˚N in 2000–2021, with observed crop data including development stages, dynamics of biomass accumulation during the growing season, final seed yields, leaf area index, and N content, enable model parameterization for effectively simulating lentil development and growth.

2 | MATERIALS AND METHODS

2.1 | Experiments and data collection

The data for model adaptation and evaluation were taken from publications and field experiments conducted at sites with contrasting environments over 2001–2022. The experiments were summarized into nine groups (Experimentd I–IX) based on the cultivars, treatments, and measurements (Table 1). Experiments I–VI were used to adapt and parameterize the lentil model and Experiments VII–IX for model validation. The locations of the experiments are shown in Figure 1.

Experiment I: Two red lentil cultivars, CDC Maxim and CDC Impulse (Maxim and Impulse hereafter), were sown on May 2, 2021, at Luskville, QC (45.46˚ N, 75.91˚ W). The soil was Orthic Humic Gleysol (Soil Landscapes of Canada Working Group, 2010) with a loam texture (15% clay, 33% silt, and 52% sand in the topsoil layer 0–30 cm). The experiment was arranged in three randomized complete blocks. The plot size was 3 m × 4 m and the field was ploughed 25-cm deep on April 12, 2021. The sowing density was 150 seeds m^{-2} with a row spacing of 30 cm. During the lentil-growing season, no fertilizer or irrigation was applied. Weeds were removed manually, and no farm chemicals were applied. Before sowing, soil samples for nine layers from 0 to 90 cm with an interval of 10 cm were taken and characterized for soil texture, soil pH, soil total N and C contents, and available soil inorganic N contents (NO_3^- and NH_4^+). Soil moisture was measured for each layer using Sentek Drill & Drop Soil Moisture Probes (https://sentektechnologies.com/products/soil-data-probes/drill-drop/) continuously during the lentil growing season. The phenological stages VE, R1, R3, R5, and R7 were recorded following nomenclature as described by Erskine et al. (1990). At R1, R3, R5, and R7 stages, leaf area index (LAI) was measured using the Digital Hemispherical Photography method (https://www6.paca.inrae.fr/can-eye/) and also with a destructive method. Around each development stage, plants in 0.18 m^2 in each plot were taken by cutting at the first node; the leaves (leaflets + petioles), stems (at R1, R3, R5, and R7), and pods (at

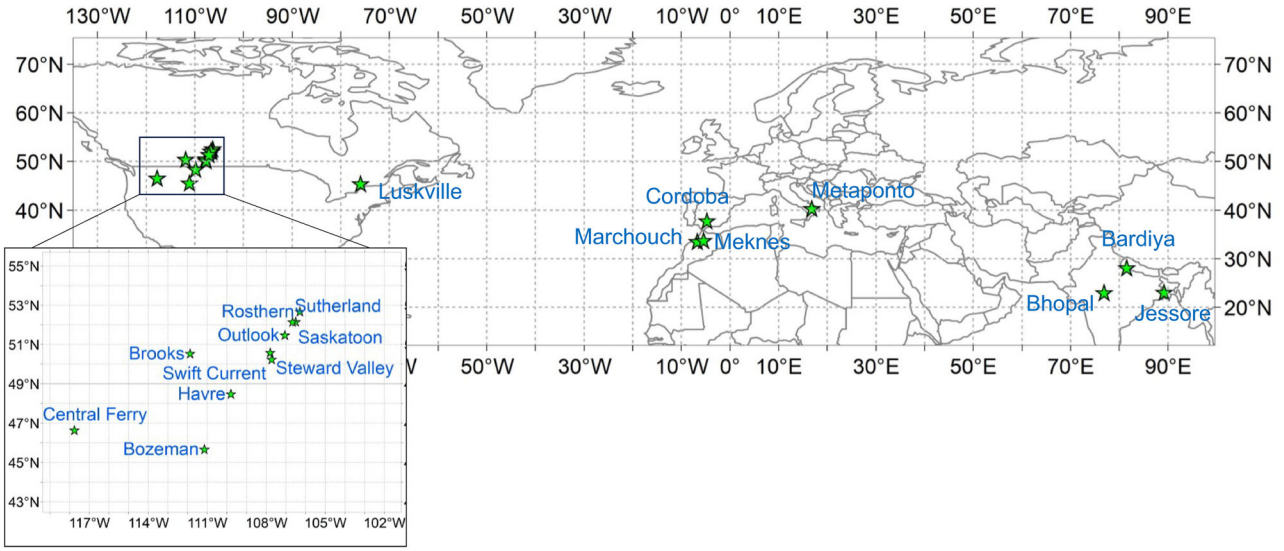

FIGURE 1 Field study sites of lentil experiments used for model development and evaluation.

R5 and R7) were separated. A subsample of green leaf was taken to measure its total area and fresh and dry biomass to calculate the specific leaf area (SLA). The leaf area was measured using ImageJ following the method described by Wang (2017). At harvest, the stems + leaves, pod shells, and seeds were separated, the pod number and the seed number per pod were recorded, and the seeds were weighed. All plant samples were dried at 70°C. Composition including N concentration (AOAC 990.03 method), lipid (AOCS Am5-04 method), lignin, carbohydrate, and minerals (wet chemistry method) were determined for each sampled plant tissue collected around R1, R3, R5, and R7. Weather data including temperature, precipitation, solar radiation, dew point, and wind speed were recorded with a weather station installed in the experimental field.

Experiment II: Three lentil cultivars, Maxim, CDC Lima (green lentil, Lima hereafter), and Impulse, were grown at Swift Current, Saskatchewan, Canada (50°15′ N, 107°44′ W) in 2021. The soil was an Orthic Brown Chernozem (Aridic Haploboroll) with silt loam texture. The first two cultivars were sown on April 27 as the early sowing treatment, on May 10 as the normal sowing, and on May 19 as the late sowing. Impulse was sown only on May 3. The experiment was arranged in four randomized complete blocks. The plots were 4 m × 8 m in size. The sowing density was 150 seeds m^{-2} with a row spacing of 25.4 cm. Monoammonium phosphate fertilizer (11-51-0) was applied at sowing with a rate of 20 kg P_2O_5 ha^{-1} and 4.73 kg N ha^{-1}. Weeds and diseases were controlled using recommended applications of the herbicide Solo ADV and fungicide Priaxor after sowing. The emergence date, flowering date, and maturity date were recorded. The biomass was sampled and measured at pre-flowering, flowering, and post flowering in 0.508 m^2 area at each plot. Five rows, that is, 10.16 m^2, were harvested to measure seed yields. Only seed yield was measured for cultivar Impulse. The biomass samples were dried at 70°C. The weather data were recorded by the weather station located within 500 m.

Experiment III: The lentil cultivar Maxim was grown in rotations with cereals and peas at Brooks (50°33′ N, 111°53′ W; elevation: 747 m), Alberta in Canada from 2011 to 2019. The soil was an Orthic Brown Chernozem with a sandy loam texture. Before the rotation experiment was initiated, wheat was grown across the site to establish a uniform background. The experiments were arranged in four randomized complete blocks. The plot sizes were 3 m × 12 m. The lentil was sown with 25-cm row spacing, generally in the first week of May every year, except in 2015, when the sowing date was June 1. The sowing density was 120 plants m^{-2}. Fertilizer providing 4–5 kg N ha^{-1} was applied as monoammonium phosphate. Weeds and diseases were controlled by herbicide Solo ADV and fungicide Priaxor after sowing. The maturity dates were recorded. At plant physiological maturity, two 1-m-long rows of lentils were randomly selected from the third row from the plot border and hand-harvested and separated into seeds and straw residue to determine seed yield, biomass yield, and seed harvest index. Details of this experiment are given in K. Liu et al. (2020). The average yield and biomass among the rotations were used for model evaluation in our study.

Experiment IV: Lentil cultivar CDC Glamis (Glamis hereafter) was grown under rainfed and irrigated conditions at Swift Current in 2006 and 2007. The soil was an Orthic Brown Chernozem (Aridic Haploboroll) of silt loam texture with 28% sand, 49% silt, and 23% clay. This experiment was designed to explore water use and distribution among varied species; thus, soil water status was measured in lysimeters installed in individual 2 m × 6 m plots of each treatment (rainfed and irrigated). The lentil density was controlled by thinning to 170 plants m^{-2} after emergence. Under the

irrigated treatment, 100 mm water was applied in 2006 and 150 mm in 2007. During the lentil growing season (early flowering, late flowering, late pod, and maturity), the plants were harvested at ground level, the number of plants per lysimeter plot was counted, and the dry weight of aboveground biomass was determined by oven drying for 3–7 days at 50°C. The weights of seed and straw at maturity were determined. Details of this experiment were reported in Gan et al. (2009).

Experiment V: The cultivar Glamis was grown at Swift Current in 2 years, 2000–2001, and at Stewart Valley, Canada (50°36′ N, 107°48′ W) in 3 years, 2000–2002. The soil was a Rego Brown Chernozem with a pH of 6.8 at Stewart Valley. The plant density was 160 seeds m^{-2} for the target plant density of 120 plants m^{-2} based on an estimated field emergence rate of 75%. The planting dates were at the end of April or early May. Each plot was 7.5 m long and consisted of eight rows with 25-cm row spacing. Fertilizer rates of 0 and 15 kg N ha^{-1} were applied at seeding. Weeds were controlled by applying herbicides. The dates of first flower and maturity were recorded. The central six rows of each plot (9.0 m^2) were harvested with a plot combine to determine seed yield. The details of the experiment can be found in Gan et al. (2005).

Experiment VI: The experimental data were from Wright et al. (2021). Two lentil cultivars, Maxim and Glamis, along with 322 other lentil cultivars were grown from 2016 to 2018 at nine sites in eight countries, including Jessore in Bangladesh, Sutherland and Rosthern in Canada, Bhopal in India, Metaponto in Italy, Marchouch in Morocco, Bardiya in Nepal, Cordoba in Spain, and Central Ferry in the United States (Figure 1). The plots were arranged in lattice squares with three replicates at each site in each year. Dates of emergence, flowering, swollen pods, and maturity were recorded. Temperatures were measured and recorded in the experiment fields. To obtain sufficient weather data to drive the model, precipitation data were obtained from Environment and Climate Change Canada (https://weather.gc.ca/canada_e.html) for the sites in Canada. Precipitation data for all other sites were obtained from the National Aeronautics and Space Administration (NASA) Langley Research Center (LaRC) Prediction of Worldwide Energy Resource (POWER) Project funded through the NASA Earth Science/Applied Science Program (https://power.larc.nasa.gov/). Daily radiation data were estimated using solar radiation at the top of the atmosphere and local daily minimum and maximum temperatures (Qian et al., 2019). The soil data were derived from SoilGrids (Poggio et al., 2021) by the geographic coordinates for the sites outside of Canada and from the Canadian Soil Information System, SLC version 3.2 (Soil Landscapes of Canada Working Group, 2010) for the sites in Canada.

Experiment VII: Eight lentil cultivars were sown at densities of 60, 100, and 140 plants m^{-2} on May 30, 2002, at Saskatoon, Canada (black soil zone) and on May 29, 2002, at Outlook, Canada (brown soil zone), with a row spacing of 14 cm. Weeds were controlled by applying herbicide and hand weeding. At Outlook, the field was irrigated with 50 mm of water in July and 25 mm in August. Biomass samples were cut at ground level from each plot on a weekly interval as two 0.3-m strips taken from two adjacent rows and oven-dried at 60°C for 3 days. Seed yield was measured by harvesting the remaining plants in the plots, and the harvested area was corrected for in-season biomass sampling. Details of the experiment and data are given in Hanlan et al. (2006). For the observed data, the in-season biomass measurements were averaged over the three population densities and five selected cultivars at Outlook. The seed yields were averaged over four adapted cultivars for each population density at both sites. The soil data were from the Canadian Soil Information System, SLC version 3.2 (Soil Landscapes of Canada Working Group, 2010). Based on the soil polygon system, the soil at Saskatoon is a clay loam soil and the soil at Outlook is a loam soil. The weather data were obtained from Environment and Climate Change Canada.

Experiment VIII: The field experiments were conducted at Montana State University's Arthur H. Post Agronomy Research Farm (PF) near Bozeman, MT (45.68° N, 111.15° W) and Northern Agricultural Research Center (NARC) near Havre, MT (48.49° N, 109.8° W) from 2019 to 2021. The soil was an Amsterdam silt loam (fine-silty, mixed, superactive, frigid Typic Haplustoll) at PF in all years. At NARC, the soil types were Telstad-Joplin loam (fine-loamy, mixed, superactive, frigid Aridic Argiustoll) in 2019 and 2020 and Kenilworth-Fort Benton fine sandy loam (fine-loamy, mixed, superactive, frigid Aridic Haplustoll) in 2021. The lentil cultivar CDC Maxim along with other nine cultivars were sown into no-till fields that contained standing cereal stubble from the previous crop at a target rate of 150 plants m^{-2}. Seeding depth was 5.1 cm at PF, and 3.2 cm at NARC. The planting dates and other management practices can be found in Baber et al. (2023). Plots were harvested with a small plot combine, and seed yield was determined on a dry matter basis. The soil textures were obtained from the soil triangle chart following the soil description, together with other soil properties from the paper (Baber et al., 2023). The weather data are derived from the POWER Project (https://power.larc.nasa.gov/) as in Experiment VI. No lentil yields were measured in 2020 due to herbicide damage and in 2021 due to poor emergence at PF.

Experiment IX: A 2-year field experiment was conducted at the research station of the National School of Agriculture in Meknes, Morocco (33.84° N, 5.48° W, and 546 m above sea level). The texture of the experimental soil was silty clay loam. The local cultivar Bekria was grown from the beginning of December to the end of May in 2020–2021 and 2021–2022 cropping seasons. Four weed control treatments were tested in four randomized complete blocks. The lentil was seeded at a depth of 3–4 cm with a density of about 100 plants m^{-2}. No chemical products or fertilizers were applied.

Irrigation and other agronomic practices were carried out over the 2 years to ensure reliable results. A total of 100 mm of water was applied in December, January, and February. The harvested yields from the treatment with the best weed control were used to evaluate the model. Soil properties were measured during the experiment. The details of the experiment and the data collected are given in Rhioui et al. (2023). The weather data were derived from the POWER Project (https://power.larc.nasa.gov/) as in Experiment VI.

2.2 | Crop model

The CSM-CROPGRO model is a generic tool that simulates crop development, daily growth, and yield using a single source code to describe the complex ecophysiological processes for diverse crops (Boote et al., 1998; Jones et al., 2003). The model template allows for parameters of species, ecotypes, and cultivar traits to be defined and input from external data files for simulations of individual crops. The CSM-CROPGRO model uses a daily time step for biomass gain but computes canopy photosynthesis at an hourly time step using leaf-level photosynthesis parameters and hedgerow light interception calculations that were described in detail by Boote and Pickering (1994). The growth rate is regulated mainly by temperature, solar radiation, and photoperiod, and includes constraints related to water and N stresses. The temperature growth factors use an average daily value that is computed from hourly temperatures. Hourly temperatures are calculated using a sine curve for temperatures during daylight hours and an exponential decay curve for decreasing temperatures from sunset to the minimum temperature. Water stress is calculated with potential and actual evapotranspiration by the latter potentially limited by soil root water uptake. The potential evapotranspiration is calculated with the Priestley–Taylor equation (Priestley & Taylor, 1972) or the FAO-56 Penman–Monteith (Allen et al., 1998). The Penman–Monteith method was selected at sites where vapor pressure and wind speed data were available; otherwise, the Priestley–Taylor equation was used in this study. The actual evapotranspiration is calculated using the LAI, a model-computed energy extinction coefficient, and root water uptake as a function of root length density and soil water content in respective soil layers (Boote et al., 2008). Nitrogen supplies come from soil N, N mobilized from plant tissues, and N assimilated through symbiotic N_2 fixation (Boote et al., 2009). Photosynthesis of sunlit and shaded leaves is computed hourly using the asymptotic exponential response equation, where quantum efficiency and light-saturated photosynthesis rate vary depending on CO_2 concentration and temperature (Boote & Pickering, 1994). The approach of Farquhar and von Caemmerer (1982) is used to calculate the response of leaf photosynthesis to CO_2. Doubling of ambient CO_2 concentration (350–700 ppm) may increase grain yield by about 30% (Boote et al., 2010). The model is generic in the sense that there is one set of code for all species, but the parameterization of the different species is specified in an extensive parameter file for species-specific traits.

2.3 | Model adaptation and parameterization

To adapt the CSM-CROPGRO model for lentils, we followed the procedures used in adapting the model for faba bean (Boote et al., 2002) and *Brassica carinata* A. Braun (Ethiopian mustard) (Boote et al., 2021). We first created the model input files based on the data collected from the experiments, including crop management, soil, and weather. Second, we adapted the crop parameter files (species, ecotype, and cultivar files) of faba bean for lentils. Third, we replaced the values of crop parameters with information found for lentil in the literature, such as tissue composition, the cardinal temperatures of processes, and the sensitivity of lentil to day length as measured in field experiments. The simulated outputs were then compared to the observed data from Experiments I–VI to fine-tune the values of crop parameters to improve the simulated precision in terms of statistical criteria between the simulated and observed crop attributes.

The model adaptation started with parameters affecting phenology and then parameters on growth, including leaf area index, total biomass accumulation, partitioning to each plant tissue, seed yield formation, and N uptake. The parameterization procedure was repeated (iterated) to minimize the gap between simulated and observed crop attributes. After accomplishing initial good calibrations of species parameters (particularly relative to composition, N mobilization, partitioning, etc.) and obtaining relatively good simulations for both time-series and the more extensive end-of-season data, the cultivar parameters were examined separately and then across each experimental site (to understand the correctness of water stress simulations and soil water traits). After final species file calibrations, we again evaluated the individual cultivar coefficients relative to biomass and seed yield (means, RMSE, simulation efficiency [EF], *d*-statistics, etc., defined below) and further adjusted the cultivar parameters to minimize the difference between the simulated and observed crop attributes.

2.4 | Model evaluation

Evaluations focused on the species parameters adapted for lentil, using the independent Experiments VII–IX (validation dataset, Table 1). In the validation sets, we used the calibrated cultivar Maxim to simulate biomass and yields in comparison with the observed values in Experiments VII and VIII,

considering that Maxim was the most widely grown cultivar in the region where those experiments were conducted. The calibrated cultivar Glamis was used for simulations in Experiment IX since its seed size is comparable to that of cv. Bekria. In addition, the use of alternative cultivars in some simulations occurred when the available data were insufficient to calibrate cultivar parameters in these experiments.

The simulated (Y) and observed (X) biomass were compared graphically. The root mean square error (RMSE) and the normalized RMSE (nRMSE, %) were calculated using Equations (1) and (2), where n is the number of observations and $\bar{X}$ is the average of observed values:

$$\text{RMSE} = \left(\frac{\sum (Y_i - X_i)^2}{n} \right)^{0.5} \quad (1)$$

$$\text{nRMSE} = \frac{\text{RMSE}}{\bar{X}} \times 100 \quad (2)$$

Model EF, mean error (ME), the relative ME (rME), and index of agreement (d) between the simulated and observed values were calculated using Equations (3)–(6).

$$\text{EF} = 1 - \frac{\sum (Y_i - X_i)^2}{\sum (X_i - \bar{X})^2} \quad (3)$$

$$d = 1 - \frac{\sum (Y_i - X_i)^2}{\sum \left(|Y_i - \bar{X}| + |X_i - \bar{Y}| \right)^2} \quad (4)$$

$$\text{ME} = \frac{1}{n} \sum_{i=1}^{n} (Y_i - X_i) \quad (5)$$

$$\text{rME} = \frac{\text{ME}}{\bar{X}} \times 100 \quad (6)$$

An optimal model was assumed to reproduce experimental data with EF and d close to 1.0, and RMSE and ME close to 0.

3 | RESULTS AND DISCUSSION

3.1 | Model parameterization and adaptation

3.1.1 | Crop development

The base temperature for development was increased from 0°C for faba bean to 2°C for lentil, deduced from McKenzie and Hill (1989). Based on the observed emergence data, the value for PL-EM (planting to emergence) was reduced from 4.8 to 1.5 photothermal time units in the ecotype file. Much of the reduction of PL-EM was caused by the use of a new soil temperature module in DSSAT V4.8, which simulates slightly lower but more accurate soil temperatures than in previous DSSAT versions. Summerfield et al. (1989a) used controlled environments to show that lentil development was accelerated under long photoperiod; thus, the model parameter PPSEN (slope of the relative response of development to photoperiod with time [positive for short-day plants]) was assumed to be negative. Summerfield et al. (1984) observed that a 16 h photoperiod accelerated lentil to flower while flowering failed under a photoperiod of 8 h, with the development rate increasing linearly with photoperiods from 10 to 16 h. McKenzie and Hill (1989) deduced that photoperiod below 7.4 h would lead to no development. In this study, the critical long day length, at which there is no delay, was parameterized between 15.4 and 16.9 h, and PPSEN was parameterized between −0.11 and −0.19 for different cultivars by optimizing to the observed lentil flowering data, together with other parameter values determining lentil development (Table 2).

3.1.2 | Crop organ composition

The model simulates the physiological processes of crop growth including N and C assimilation and maintenance respiration, which requires values of the related tissue compositions of respective organs. Uptake of N depends on N availability in the soil and on the plant N demand, which is a function of rate of dry matter gain and target N concentration of the different organs. When root N uptake is insufficient to meet plant N demand, assimilate is directed to nodule growth and biological N_2 fixation for legume species. To simulate these processes, the tissue compositions for each plant organ are required, along with target N concentrations.

The parameterized leaf protein concentrations are listed in Table 3 and were based on observed values and data from the literature. Our values were slightly lower than the values reported by Zakeri et al. (2015), in which leaf N concentration ranged from 3.6% to 4.9% with an average of 4.4% in the vegetative phase, 3% to 4.7% and an average of 4.0% at the first pod, and 1.8% to 4.1% and an average of 2.8% at the late pod phase. Seed N concentration was reported to range from 4.0% to 4.4% for five cultivars under 0–60 kg N ha^{-1} treatments, and there were no differences between small- and large-green seed classes (Zakeri, Bueckert, et al., 2012; Zakeri, Lafond, et al., 2012). Literature on lentil seed composition shows that lentil seed has 28.6% protein, 3.1% ash, 4.9% crude fiber, and <1% ether extract (Bhatty, 1988). From this information, the composition for the various plant organs was parameterized (Table 3). The other compositions including fractions of carbohydrate-cellulose, lipid, lignin, and minerals were estimated from the aforementioned experiments and the literature (Table 3). Detailed descriptions of the function of the composition parameters are given in Boote et al. (2002, 2021).

TABLE 2 Cultivar coefficients for four lentil cultivars after calibration and as compared to default values for faba bean.

Parameter	Definition	Faba bean	Maxim	Glamis	Lima	Impulse
CLDL	Critical long day length (h)	24.0	15.8	15.4	16.9	16.0
PPSEN	Slope of the relative response of development to photoperiod with time (h^{-1})	−0.031	−0.11	−0.11	−0.19	−0.11
EM-FL	Time between plant emergence and flower appearance (R1) (photothermal days)	18.0	26.5	28.0	23.0	29.0
FL-SH	Time between first flower and first pod (R3) (photothermal days)	10.9	7.5	5.0	5.0	7.5
FL-SD	Time between first flower and first seed (R5) (photothermal days)	24.0	10.0	8.0	8.0	11.0
SD-PM	Time between first seed (R5) and physiological maturity (R7) (photothermal days)	34.5	21.0	22.5	20.0	18.5
FL-LF	Time between first flower (R1) and end of leaf expansion (photothermal days)	45.0	20.0	16.0	18.0	15.0
LFMAX	Maximum leaf photosynthesis rate at 30°C, 350 vpm CO_2, and high light (mg CO_2 m^{-2} s^{-1})	1.00	1.00	0.86	0.90	0.83
SLAVR	Specific leaf area of cultivar under standard growth conditions (cm^2 g^{-1})	285	220	240	220	230
SIZLF	Maximum size of full leaf (cm^2)	110	70	70	70	70
WTPSD	Maximum weight per seed (g)	1.100	0.044	0.065	0.065	0.065
SFDUR	Seed filling duration for pod cohort at standard growth conditions (photothermal days)	21.0	20.0	20.0	20.0	20.0
SDPDV	Average seed per pod under standard growing conditions (#/pod)	2.4	1.3	2.0	2.0	1.3
PODUR	Time for cultivar to reach final pod load under optimal conditions (photothermal days)	18.0	14.0	14.0	16.0	18.0
THRSH	The maximum ratio of seed/(seed + shell) at maturity	77.0	69.0	67.0	68.0	60.0
SDPRO	Fraction protein in seed (g g^{-1})	0.315	0. 286	0. 286	0. 286	0. 286
SDLIP	Fraction lipid in seed (g g^{-1})	0.020	0.020	0.020	0.020	0.020
PL-EM(eco)[a]	Time between planting and emergence (photothermal days)	4.8	1.5	1.5	1.5	1.5
EM-V1(eco)	Time from emergence to first true leaf (V1), (photothermal days)	4.0	2.8	2.8	2.8	2.8
TRIFOL(eco)	Rate of appearance of leaves on the mainstem (leaves per thermal day)	0.35	0.35	0.35	0.35	0.35
LNGSH(eco)	Time required for growth of individual shells (photothermal days)	15	14	14	14	14

[a]eco, parameters in ecotype file, the other parameters in cultivar file.

3.1.3 | Leaf N mining parameters

Simulated leaf N concentration initially did not decline as rapidly as observed in Experiment I, thus we increased N mobilization rates NMOBMX (relative rate per day) and NVSMOB (rate during vegetative phase as a fraction of NMOBMX). This was done iteratively by modifying leaf protein, LFMAX (maximum leaf photosynthesis rate), late-season seed growth, and the rate of leaf and petiole abscission (the latter two depend on N mobilization). In Experiment I, the soil had high N fertility (high initial soil N), so N-fixation was not required, and leaf N concentration attained high values because the model considers uptake of "luxury" available N. Final values for NMOBMX and NVSMOB were 0.115 and 0.50, respectively (Table 3), which are higher than 0.074 and 0.35 for faba bean but closer to values for soybean. Faster mobilization was expected because of the shorter life cycle of lentil compared to faba bean. In the future, these parameter estimates could likely be improved using tissue samples from field experiments where indigenous soil N was low enough to promote N-fixation.

3.1.4 | Leaf photosynthesis

Literature values for leaf photosynthesis rate ranged from 18 to 24 μmol CO_2 m^{-2} s^{-1} (equivalent to 0.79–1.06 mg CO_2 m^{-2} s^{-1}) among eight genotypes under well-watered conditions (Sehgal et al., 2017). The LFMAX was initialized at 0.80 mg CO_2 m^{-2} s^{-1}, and in subsequent calibrations,

TABLE 3 The parameterized values for crop attributes including organ tissue composition and temperature parameters in species file used for CROPGRO-Lentil model, compared to default values used for CROPGRO-Faba Bean.

Parameter	Definition	Faba bean	Lentil
PROLFI (g g^{-1})	Leaf protein fraction—luxury	0.344	0.210
PROLFG (g g^{-1})	Leaf protein fraction—growth	0.294	0.158
PROLFF (g g^{-1})	Leaf protein fraction—final	0.112	0.112
PROSTI (g g^{-1})	Stem protein fraction—luxury	0.150	0.170
PROSTG (g g^{-1})	Stem protein fraction—growth	0.100	0.132
PROSTF (g g^{-1})	Stem protein fraction—final	0.050	0.050
PROSHI (g g^{-1})	Shell protein fraction—luxury	0.220	0.150
PROSHG (g g^{-1})	Shell protein fraction—growth	0.220	0.071
PROSHF (g g^{-1})	Shell protein fraction—final	0.080	0.040
SDPROS (g g^{-1})	Seed protein fraction at 25˚C of standard cultivar	0.325	0.286
PCARLF (g g^{-1})	Proportion of leaf carbohydrate/cellulose	0.417	0.587
PCARST (g g^{-1})	Proportion of stem carbohydrate/cellulose	0.664	0.616
PCARRT (g g^{-1})	Proportion of root carbohydrate/cellulose	0.703	0.715
PCARSH (g g^{-1})	Proportion of shell carbohydrate/cellulose	0.410	0.633
PCARSD (g g^{-1})	Proportion of seed carbohydrate/cellulose	0.575	0.640
PLIPLF (g g^{-1})	Proportion of leaf lipid	0.025	0.028
PLIPST (g g^{-1})	Proportion of stem lipid	0.020	0.010
PLIPRT (g g^{-1})	Proportion of root lipid	0.020	0.005
PLIPSH (g g^{-1})	Proportion of shell lipid	0.020	0.008
PLIPNO (g g^{-1})	Proportion of nodule lipid	0.050	0.010
PLIGLF (g g^{-1})	Proportion of leaf lignin	0.070	0.055
PLIGST (g g^{-1})	Proportion of stem lignin	0.070	0.100
PLIGSH (g g^{-1})	Proportion of shell lignin	0.280	0.114
PLIGSD (g g^{-1})	Proportion of seed lignin	0.015	0.010
POASD (g g^{-1})	Proportion of seed organic acid	0.030	0.013
PMINLF (g g^{-1})	Proportion of leaf mineral	0.094	0.070
PMINST (g g^{-1})	Proportion of stem mineral	0.046	0.054
PMINRT (g g^{-1})	Proportion of root mineral	0.057	0.060
PMINSH (g g^{-1})	Proportion of shell mineral	0.030	0.055
PMINSD (g g^{-1})	Proportion of seed mineral	0.035	0.031
NMOBMX	Maximum fraction of N that can be mobilized in a day	0.074	0.115
NVSMOB	Rate during vegetative phase as a fraction of NMOBMX	0.035	0.50
SLWREF (g cm^{-2})	The specific leaf weight at which light-saturated leaf photosynthesis is defined	0.0034	0.0038
SLAMAX (cm^2 g^{-1})	Maximum SLA, the thinnest leaf at extreme low light	900	450
SLAMIN (cm^2 g^{-1})	Minimum SLA, the thickest leaf at saturating solar radiation at optimum temperature with no water stress	325	156
SLAREF (cm^2 g^{-1})	SLA for new leaves during peak vegetative growth for the standard cultivar	285	220
DWNODI (g $plant^{-1}$)	Initial nodule weight	0.03	0.01
NODRGM (g g^{-1} day^{-1})	Relative growth rate of nodules	0.22	0.22
CMOBMX	Maximum C pool mobilization rate, fraction of available carbohydrate pool per day	0.03	0.04
PORPT	Fraction of petiole to leaf mass	0.15	0.20
SENRTE (g g^{-1})	Amount of "N-exhausted" leaf mass per unit of N mobilized	0.8	0.9
SENRT2 (day^{-1})	Rate of leaf and petiole abscission per calendar day after physiological maturity	0.15	0.18
YRTFAC (cm)	Maximum rate of root depth progression per photothermal day	2.6	2.3
T_b (˚C)	The base temperature for crop development	0	2

(Continues)

TABLE 3 (Continued)

Parameter	Definition	Faba bean	Lentil
FNNGT(4) or FNFXT(4) (°C)	Temperature curve describing relative nodule growth rate or N-fixation rate versus soil temperature	1, 16, 25, 40	0, 14, 25, 40
FNPGL(4) (°C)	Temperature curve describing effect of T_{min} on leaf photosynthesis rate	−2, 14, 50, 60	−2, 11, 50, 60

Abbreviation: SLA, specific leaf area.

it was increased to cultivar-dependent values in the middle of the reported range. These values are slightly lower than expected compared to other legumes such as soybean and dry bean, but cultivar values can be modified as needed. Respective values for Maxim, Glamis, Lima, and Impulse were optimized at 1.00, 0.86, 0.90, and 0.83 mg CO_2 m^{-2} s^{-1} (Table 2). The specific leaf weight at which light-saturated leaf photosynthesis is defined (SLWREF) was increased from 0.0034 to 0.0038 g cm^{-2} for lentil (Table 3). The slightly higher value for lentil causes lower productivity compared to faba bean. Temperature parameterization of instantaneous photosynthesis (T_b, base temperature = 1°C and T_{opt}, optimum temperature = 30°C) based on the faba bean model was accepted and appeared to be adequate. Later, during the evaluation of site effects, we found that the prior night temperature (T_{min}) was relatively lower in Experiment III in some years than for other locations, and those cool seasons also had lower simulated yields than the observed. Thus, the effect of T_{min} on leaf photosynthesis was modified from −2 and 14°C (asymptotic response from zero rate to full rate) to −2 and 11°C, which improved model performance (Table 3).

3.1.5 | Specific leaf area

The simulated SLA of new, daily-produced leaves is controlled by the daily solar radiation level, a temperature function, and water stress. The temperature parameterization was made slightly more sensitive than that of faba bean with a T_b of −2.5°C and a T_{opt} of 20.0°C. The water stress impacts on SLA were retained from faba bean. The effect of solar radiation on SLA is set by SLAMAX (maximum SLA, the thinnest leaf at extreme low light) and SLAMIN (minimum SLA, the thickest leaf at saturating solar radiation but still at optimum temperature with no water stress). The final SLAMAX and SLAMIN values were set at 450 and 156 cm^2 g^{-1}, respectively (Table 3). The SLAREF (SLA for new leaves during peak vegetative growth for the standard cultivar) and SLAVR (specific leaf area of cultivar under standard growth conditions) were both set to 220 cm^2 g^{-1}. Using SLAREF and SLAVAR of 220 cm^2 g^{-1} has no effect on the simulations since they normalize each other, unless SLAVAR is different for a given cultivar compared to the standard cultivar. In this case, Maxim was considered the standard cultivar with SLAVAR of 220 cm^2 g^{-1}, and the values of SLAVAR for Glamis, Lima, and Impulse were set at 240, 220, and 230 cm^2 g^{-1} (Table 2). Experiment I was the only one where SLA was measured, with values averaging 180 cm^2 g^{-1}, which math included petioles with leaflets. The SLAMAX and SLAMIN were adjusted such that the simulations came close to the observed SLA for that experiment. Additional reasons for setting the SLA to somewhat lower values were to come closer to the LAI of the other treatments (for which SLA was not measured) and because lower LAI reduced transpiration, which was needed for the rainfed experiments including Experiment III at the Brooks site. There were no water deficit conditions for Experiment I, which limited testing of water deficit-induced reductions in LAI or SLA. Our estimates for SLA parameters were consistent with the reported values that ranged from 179 to 256 cm^2 g^{-1} with a median value of 206 cm^2 g^{-1} that were measured in experiments with eight lentil cultivars grown in Saskatchewan in Canada (Zakeri et al., 2015). It is noted that the leaf area was measured using a leaf area meter (Model LI-3100C) in their experiments rather than the ImageJ method in our Experiment I. Nevertheless, the measured SLA values in the two experiments should be comparable because little difference was found between these two methods in measuring crop leaf area (Martin et al., 2020).

3.1.6 | Nodule growth, N fixation, and its temperature dependence

Initial nodule weight (DWNODI) was reduced from 0.03 to 0.01 g $plant^{-1}$ (Table 3), a value about one-third that of soybean. Nodule relative growth rate (NODRGM) was unchanged from faba bean. The temperature dependence (T_b and first T_{opt}) of nodule (relative) growth rate and of specific nitrogenase activity was reduced from 1.0 and 16.0°C to 0.0 and 14°C (FNNGT(4); Table 3), also with a shift from a linear (LIN) lookup to asymptotic lookup (QDR). Both the temperature parameterization and the change to QDR reduced the sensitivity of nodule growth and N fixation to low soil temperature required for the cooler Canadian sites. This modification was also associated with the newly parameterized soil temperature module because, for comparison, the present faba bean model with the new soil temperature function assumes T_b of 1.0 and first T_{opt} of 14°C.

TABLE 4 Partitioning to leaf (YLEAF), stem (YSTEM), and root among vegetative tissues as a function of main stem leaf number (XLEAF) in lentil species file.

XLEAF/leaf No.	0.0	1.8	1.4	6.0	8.5	10.5	15.0	40.0	Final
YLEAF/to leaf	0.54	0.54	0.53	0.45	0.38	0.18	0.18	0.18	0.18
YSTEM/to stem	0.07	0.18	0.21	0.37	0.39	0.55	0.58	0.58	0.58
Rest to root	0.39	0.28	0.26	0.18	0.23	0.27	0.24	0.24	0.24

Note: Transition to "Final" begins at flowering. Roots receive (1.00-YLEAF-YSTEM). Reproductive growth takes priority, so vegetative growth will go to zero when a full pod-load is set.

TABLE 5 The parameterized values for the length of internode per node (YVSHT) and the increase in canopy width per node (YVSWH) depending on the node number (XVSHT) on lentil main stem.

XVSHT	0	1	4	6	8	10	14	17	22	40
YVSHT (m)	0.0135	0.0158	0.0218	0.034	0.0365	0.0376	0.0343	0.0288	0.0188	0.0055
YVSWH (m)	0.0141	0.0158	0.0212	0.0285	0.0282	0.0282	0.0255	0.0200	0.0100	0.0022

Note: The main stem node appearance is temperature dependent.

3.1.7 | Partitioning to leaf, stem, and root

Parameter values for assimilate partitioning were accomplished with minimal available data on leaf, stem, and total shoot mass for two cultivars in Experiment I and root mass for two treatments in two growing seasons in Experiment IV. Partitioning function values (Table 4) differed considerably from those of faba bean. We consistently found it necessary to increase allocation to leaf tissue during most of the crop cycle and to reduce the allocation to stem later in the life cycle, but to increase allocation to root (Table 4).

3.1.8 | Canopy height and width

No observational data were available for canopy height or width, and those dimensional characteristics can impact the canopy envelope for light interception, especially when considering variation in row spacings. We targeted an end-season height of 44–53 cm. To simulate canopy height and width over time, we modified the canopy height and width extension parameters: length of internode per node (YVSHT) and the increase in canopy width per node (YVSWH) as a function of main stem node number (XVSHT) (Table 5). Rates of canopy height and width increase are strongly dependent on V-stage (XVSHT) progression, which depends on temperature. In addition, the height and width functions are multiplied by RHIGHT and RWIDTH, which were set to 1.0 (to allow for cultivar differences in canopy height and width).

3.1.9 | Minor adaptations in the species file

The value of CMOBMX (maximum C pool mobilization rate) was increased from 0.03 to 0.04 (relative rate per day; Table 3) to accelerate the mobilization of stored total nonstructural carbohydrates (TNC) pools from leaf and stem to seed. This improved simulations slightly, reducing leaf, stem, and vegetative mass late in life cycle while increasing final pod and seed mass. This also appeared to improve the final TNC concentration of leaf and stem, although observed values were not available for comparison.

The parameter for petiole as a fraction of leaf mass (PORPT) was increased from 0.15 to 0.20 (Table 3). This parameter is used to mimic the loss of stem mass (i.e., petioles) from the plant as leaves abscise. Measured values on the fraction of stem mass including petioles were lacking, as well as data to assess the rate of leaf abscission. This can be improved if data are available. The SENRTE value (amount of "N-exhausted" leaf mass per unit of N mobilized) was increased from 0.80 to 0.90 to reduce leaf mass during late reproductive growth. The SENRT2 value (rate of leaflet and petiole abscission per calendar day after physiological maturity) was increased from 0.15 to 0.18, again to reduce final top (minus pod and seed) mass at harvest maturity. The rate of root depth progression (YRTFAC) was reduced from 2.6 to 2.3 cm per photothermal day. The water stress-induced acceleration of final maturity was reduced from 1.00 to 0.70 (0.70 is the value for soybean).

The duration of growth of individual shells (LNGSH) in the ecotype file was reduced from 15 to 14 photothermal days. This change had a minor impact, but 15 photothermal days seemed excessive as compared to 10 photothermal days for soybean.

3.1.10 | Cultivar calibration

Important modifications to cultivar parameters included reducing threshold phases for FL-SH, FL-SD, and SD-PM as compared to values for faba bean defaults, based on timing to

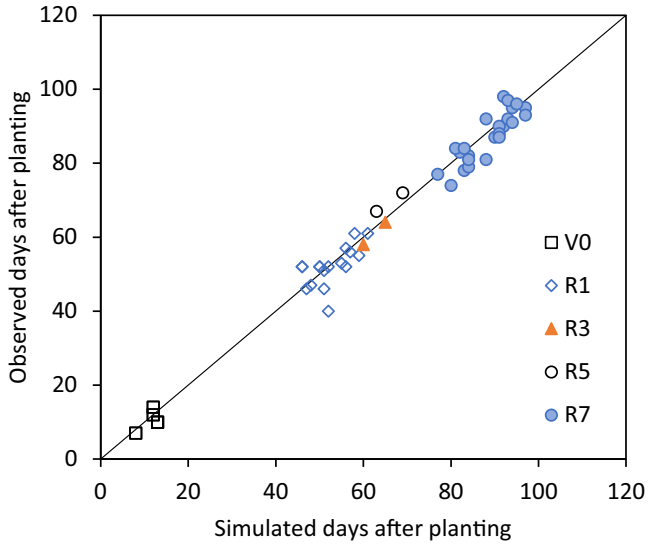

FIGURE 2 Comparison of observed versus simulated phenology for lentils at sites in Experiments I–V. Growth stages are days from planting to emergence (V0), early bloom (R1), early pod (R3), early seed (R5), and physiological maturity (R7). Experiment details are given in Table 1.

the beginning pod growth, time to maturity, and the shorter life cycle of lentil compared to faba bean (Table 2). In addition, the pod adding duration (PODUR), and in some cases, the single seed growth duration (SFDUR) were reduced. These two modifications tended to increase yield for similar levels of biomass accumulation. The leaf photosynthesis parameter LFMAX was modified early in the calibration, and the cultivars were individually distinguished by minor changes in LFMAX. Another key modification based on sparse data was to reduce the default threshing percentage (THRESH) for faba bean of 77% to values between 60% and 69% depending on the cultivar. The reference weight per seed (WTPSD) was calibrated as 44 mg for Maxim to 65 mg for Glamis and Lima. The calibrated seed weight for Glamis is comparable to the reported values for this cultivar (Gan et al., 2005).

3.2 | Model performance

3.2.1 | Simulations of crop development

The simulated and observed phases for the phenological stages of V0 to R7 are graphically compared in Figure 2 for Experiments I–V and Figure 3 for Experiment VI. The values for the days to each development stage of emergence and R1–R7 are concentrated around the line of 1:1 relationship between the simulated and observed values in Experiments I–V (Figure 2), indicating that the development of lentil was well simulated in these experiments. The statistical criteria showed a high similarity between the simulated and observed values with a mean error of 1 day and an RMSE of 4 days (Table 6). For Experiment VI, the RMSE (11 days) was much higher than those for Experiments I–V, which was caused by large deviations at Bardiya, Nepal. These simulated deviations occurred for each development stage at Bardiya, with underestimated days to each development stage (Figure 3), as shown by the points located far from the 1:1 line. If the data in Nepal were excluded, the statistical criteria showed the comparable values to those for Experiments I–V. For the experiment in Nepal, the simulated phase for emergence was much shorter than observed. To test if the simulated deviations existed for lentil development after emergence at this site, we aligned the emergence dates to the observed by modifying crop planting dates in the model input file. The simulations for the subsequent development stages were improved, but the days to each development stage were still underestimated. Underestimation of the days to each development stage at the Nepal site was also noted by Wright et al. (2021) using their phenology model. They argued that there might be other factors influencing the development rates. Considering that the difference was not readily explained by the factors considered in the CSM-CROPGRO model and the limited information available associated with this set of data, further data, such as seeding depth, soil properties, soil temperature and moisture, and local exact rainfall data, may be required to understand why the model underestimated days to each development stage at this site.

3.2.2 | Simulations of LAI

Detailed data were measured in Experiment I, including the growth dynamics of LAI and biomass for each plant tissue during the lentil growing season. With the properly parameterized SLA, the simulated SLA values were comparable to the observed values for cultivars Maxim and Impulse (Figure 4). The simulated LAIs also matched well to the measured LAIs for these two cultivars. Statistical analysis showed that the simulations on LAIs were efficient with RMSE = 0.46 and ME = 0.1.

3.2.3 | Biomass

The dynamics of total aboveground biomass were simulated with patterns similar to those observed during the growing season for cultivars Maxim and Impulse in Experiment I (Figure 5). The observed mass of leaves and stems was also close to simulated values, but the pod mass was overestimated for both cultivars.

In Experiment II at Swift Current (Figure 6), the growing season was longest under early seeding and the duration

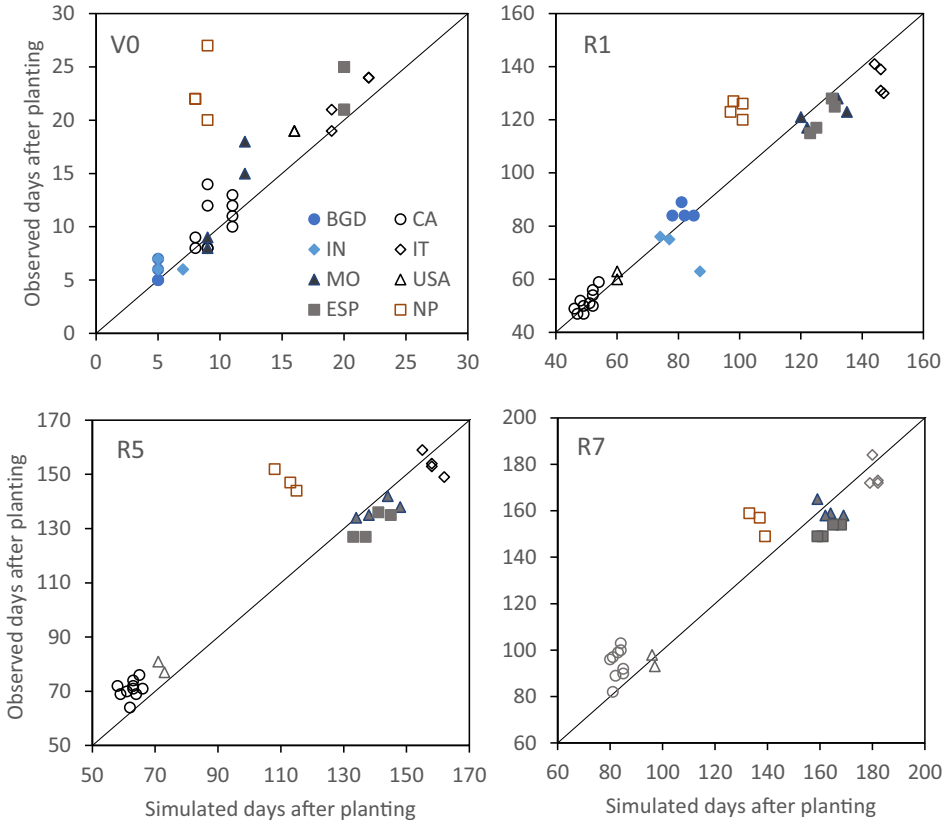

FIGURE 3 The observed versus simulated days from planting to emergence (V0), early bloom (R1), early seed (R5), and physiological maturity (R7) for lentil cultivars Maxim and Glamis across eight countries in Experiment VI. BGD: Bangladesh, CA: Canada, IN: India, IT: Italy, MO: Morocco, USA: United Sates, ESP: Spain, NP: Nepal.

TABLE 6 Summary statistics for comparison of observed and simulated growth stages as days after planting for six experiments used to parameterize the CSM-CROPGRO-Lentil model.

	No.	X_{obs}	X_{sim}	RMSE	nRMSE (%)	*d*	EF	ME	rME (%)
I–V	61	66	67	4	5.9	0.99	0.98	1	1.3
VI	123	82	79	11	13.2	0.99	0.96	−3	−3.4

Note: No.: number of measured/simulated data pairs; X_{obs}: mean of observed days; X_{sim}: mean of simulated days; RMSE: root mean square error between simulated and observed days; nRMSE: normalized RMSE; *d*: index of agreement; EF: model simulation efficiency; ME: mean error (day); rME: relative ME.

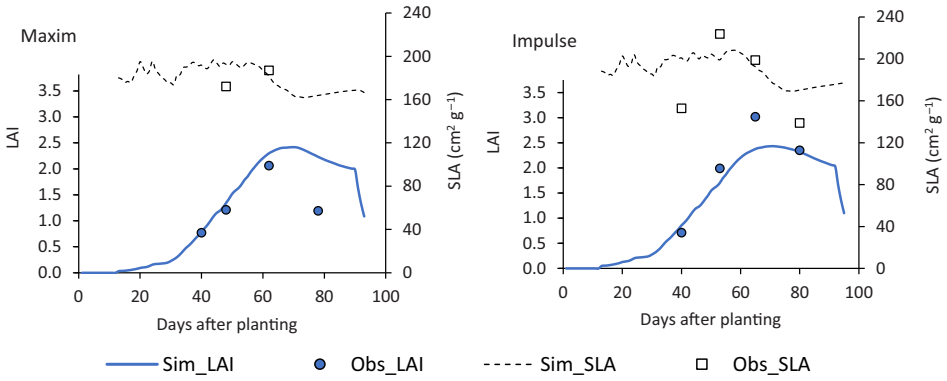

FIGURE 4 Simulated and observed values of leaf area index (LAI) and specific leaf area (SLA) for two cultivars Maxim and Impulse at Luskville, Quebec, Canada, in 2021 (Experiment I).

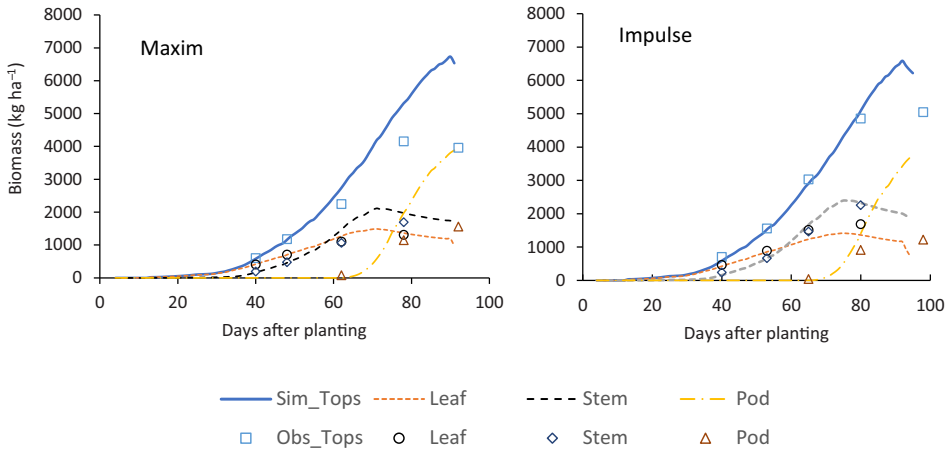

FIGURE 5 The simulated and observed total aboveground biomass (Tops), leaf, stem, and pod of two cultivars Maxim and Impulse at Luskville, Quebec, Canada, in 2021 (Experiment I).

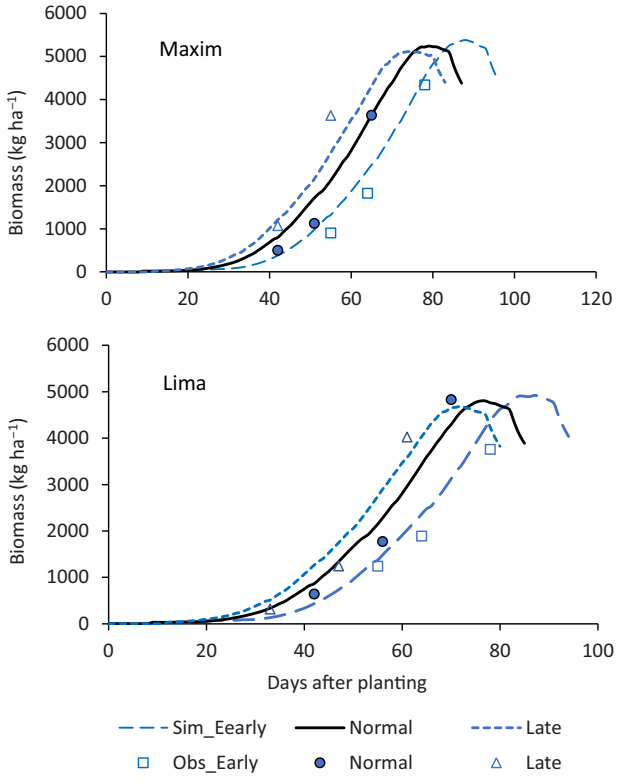

FIGURE 6 Simulated values and observed values of total aboveground biomass for two cultivars Maxim and Lima at three sowing dates at Swift Current, Canada, in 2021 (Experiment II).

of biomass accumulation was shortest under the late seeding treatment. The differences in biomass accumulation curves were well simulated by the model for both cultivars Maxim and Lima. The good simulations of the dynamics of biomass accumulation were indicated by the statistical criteria, that is, nRMSE = 20.2%, d = 0.98, and EF = 0.92 (Table 7).

The model simulated the impacts of water deficits on biomass accumulation. In Experiment IV at Swift Current (Figure 7), simulated biomass accumulation was greater for the irrigated lentil than the rainfed treatment in both years, and the simulated dynamics of total aboveground biomass were close to the observed values except for the final total aboveground biomass of the irrigated lentil in 2007. The simulated root biomass was also close to the observed values. The simulated root biomass of irrigated lentil was only slightly larger than that of the rainfed lentil late in the growing season, and small differences were observed between irrigated and rainfed lentil (Figure 7).

Overall, the model captured the dynamic accumulation of total aboveground biomass for different lentil cultivars, sowing dates, and irrigation treatments in the calibration dataset. The comprehensive statistical criteria for total biomass showed that the model successfully simulated the dynamics of biomass with nRMSE = 19.9%, d = 0.98, and EF = 0.92 (Table 7).

In Experiment III, the simulated total biomass at harvest was close to the observed values except for 2012, when biomass was underestimated (Figure 8). In these simulations, water deficits were likely small as rainfall appeared to be sufficient (191 mm of rainfall vs. 214 mm of potential evapotranspiration) from emergence to maturity. The underestimation of biomass in 2012 suggests that there might be some information not available to be incorporated into the model input files. Despite the underestimation of biomass in 2012, overall, statistical criteria showed that the final biomass was well reproduced with nRMSE = 19.1%.

In Experiment VII, which served as an independent evaluation dataset, the simulated accumulations of aboveground biomass were close to the observed values (Figure 9). The statistical criteria indicated satisfactory simulation of the biomass accumulations with nRMSE = 22%, d, and

TABLE 7 Summary statistics for comparisons of observed and simulated accumulation of aboveground biomass for three experiments used to parameterize the CSM-CROPGRO-Lentil model and one experiment used to provide independent validation.

Experiment	No.	X_{obs}	X_{sim}	RMSE	nRMSE (%)	*d*	EF	ME	rME (%)
Calibration set									
I	10	2734	3238	913	33.4	0.94	0.68	504	18.4
II	18	2056	2311	416	20.2	0.98	0.92	255	12.4
IV	15	3169	3528	614	19.4	0.93	0.77	360	11.4
Total	43	2602	2894	517	19.9	0.98	0.92	292	11.2
Validation set									
VII	6	2406	2886	537	22.3	0.96	0.84	480	20.0

Note: No.: number of measured/simulated data pairs; X_{obs}: mean of measured biomass (kg ha^{-1}); X_{sim}: mean of simulated biomass (kg ha^{-1}); RMSE: root mean square error between simulated and measured biomass (kg ha^{-1}); nRMSE: normalized RMSE; *d*: index of agreement; EF: model simulation efficiency; ME: mean error (kg ha^{-1}); rME: relative ME.

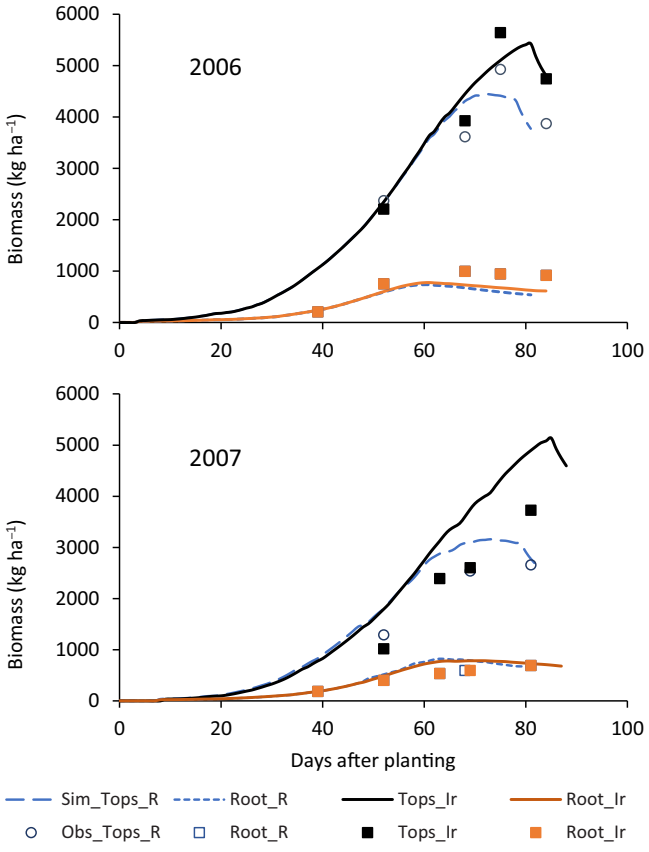

FIGURE 7 The simulated and observed values of total above ground biomass (Tops) and root biomass of Glamis under rainfed (R) and irrigated (Ir) conditions at Swift Current, Canada, in 2006 and 2007 (Experiment IV).

EF > 0.84 (Table 7). In the simulations, the calibrated cultivar Maxim was used as a generic cultivar rather than five individual cultivars used in the experiments due to insufficient data from the literature (Hanlan et al., 2006). Biomass dynamics could likely be simulated more accurately if individual cultivars were calibrated using observed data. Overall, simulation of the biomass dynamics indicated that the model had been successfully adapted to lentil.

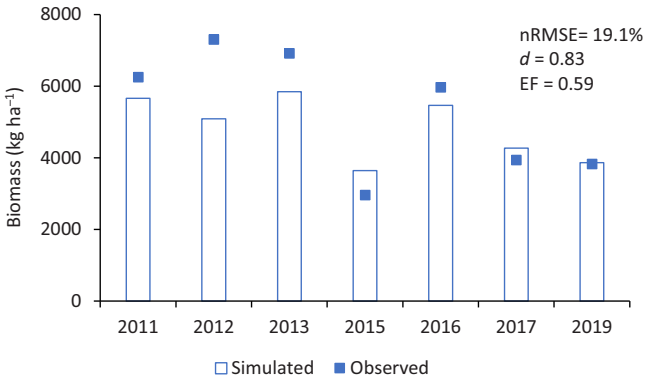

FIGURE 8 The simulated versus observed biomass at harvest for Experiment III that are detailed in Table 1.

3.2.4 | Seed yield

The adapted model generally simulated lentil yields well across Experiments I–V as most of the points are concentrated around the 1:1 line except for four points that are relatively far from the 1:1 line (Figure 10A). The overestimated yields occurred in Experiment I, and the underestimated simulations occurred in Experiment III in 2011 and 2012. The low observed lentil yields in Experiment I were associated with low harvest index (0.13–0.27), which was likely caused by excessive vegetative growth of lentil in a humid region. This is despite a good time-series simulation of LAI, leaf, stem, and total biomass. These low seed yield and harvest index (HI) may indicate poor adaptation of the selected lentil cultivars to this site. Whitehead et al. (2000) reported a similar low HI and excessive vegetative growth in Reading, UK, under relatively cool and wet conditions. During Experiment I, adequate rainfall combined with a fertile soil may have led to excessive vegetative growth. Lake and Sadras (2021) reported that such growth usually leads to self-shading, reduced pod and seed set, low harvest index, and higher risk of disease and lodging. In addition, recommendations for commercial

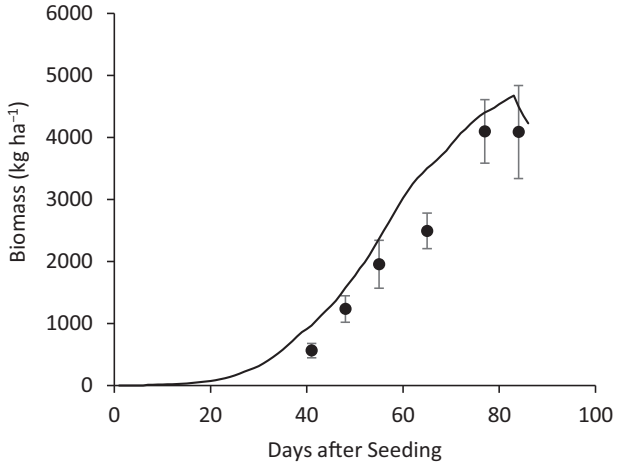

FIGURE 9 The simulated (solid line) and observed (symbols) values of total above ground biomass at Outlook, Canada, in 2002 (Experiment VII). The simulated values are for cultivar Maxim and the observed values are the average of five cultivars used in the experiment, the vertical bars are the standard deviations among cultivars.

lentil production suggest that lentil has moderate resistance to water deficits, but that high moisture promotes excessive vegetative growth, reduces seed yield, and aggravates disease problems (https://albertapulse.com/growing-lentils/). It is also possible that the surplus soil N supply at the Luskville site, which is known to promote excessive vegetative growth in crops like cotton, contributed toward the low harvest index. The mechanisms of the excessive vegetative growth of lentil leading to low HI need to be further explored to improve the model's ability for evaluating the adaptability of lentil to specific regions.

The underestimation of yield in 2012 in Experiment III was consistent with the underestimated biomass. In Experiment III in 2011, the dry condition with less rainfall (160 mm) during the growing season seemed to favor an increase in the number of pods and seeds, which led to a higher harvested yield, confirming the need to further explore the mechanisms of lentil yield formation to improve the model. Except for the very high nRMSE caused by overestimated yields in Experiment I, the values of nRMSE were comparable to the performance of the CSM-CROPGRO model for simulating the seed yields of other species with nRMSE from 14% to 22% (Boote et al., 2021; Jing et al., 2016).

In the validation set, the observed versus simulated yields were concentrated around the 1:1 relationship between the simulated and observed values, except for one point relatively far from the 1:1 line (Figure 10B). The overestimated yield occurred at NARC in 2019, when the yield was expected to be similar to 2020, with comparable precipitation between these 2 years (158 vs. 140 mm) during the growing season. The cause for the much lower observed yield was not indicated in the paper (Baber et al., 2023). Overall, the statistical criteria showed a good yield simulation with nRMSE = 19%, $d = 0.91$, and EF = 0.71 (Table 8). Considering that the cultivar was not calibrated for each experiment, the simulated yields being already close to the observed data indicates a successful model adaptation to simulate lentil seed yield.

3.2.5 | Perspectives for further improving model performance

We are encouraged by the promising performance of this model in simulating the development and growth of spring lentil. Nevertheless, there are several avenues to improve the model to meet its diverse application purposes and to gain new insights into the ecophysiology of the lentil crop. The following issues should be considered in future lentil model coding and parameters to make it more robust for future use:

1. The underlying mechanisms of excessive vegetative growth need to be explored further and simulated in the model for evaluating the adaptability of lentils to specific regions. While we hypothesize the cause may be humid environments that contribute to excessive vegetative growth, which leads to low seed number and low harvest index, it is also possible from other environmental factors, including excessive available soil inorganic N or high temperature.
2. The model should be further improved for simulating seed quality (protein and oil content). This requires access to extensive data on those quality aspects across multiple environments, including temperature, water, and N variation.
3. Although some physiological parameters such as SLAVAR were parameterized according to our measured data, others, such as LFMAX and cardinal temperatures, were derived from the literature or adapted from those for faba bean due to the limited available measured data, which may reduce the reliability and robustness of the simulation. These physiological parameters, such as leaf photosynthesis of lentil under favorable growing condition, may be further improved based on measured values to increase the simulation mechanism of this lentil model in the future. The values of cardinal temperatures may potentially be improved by further testing of temperature effects on development and growth, which is critical for climate change, and by introducing lentil into novel regions.
4. Model development is focused on lentils with a spring growth habit, requiring no vernalization or winter dormancy processes. From preliminary simulations of winter lentil in the Supporting Information with the calibrated parameters (Table S1), the present adapted model simulated well the phenological development (Figure S1) and

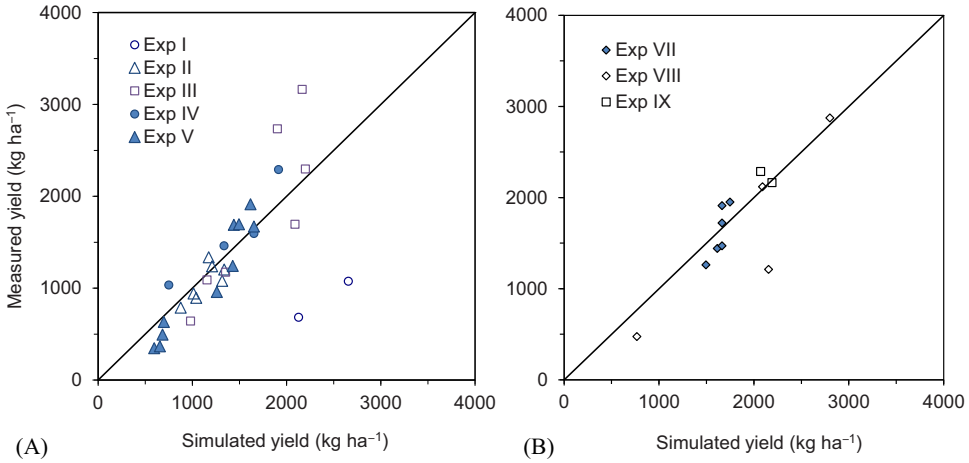

FIGURE 10 Comparison of measured versus simulated seed yields for Experiments I–V (A) used for model development and parameterization, and Experiments VII–IX (B) used for model evaluation (validation set). Experiment details are given in Table 1.

TABLE 8 Summary statistics for comparisons of observed and simulated seed yield for five experiments used to parameterize the CSM-CROPGRO-Lentil model and three experiments used to provide independent validation.

Experiment	No.	X_{obs}	X_{sim}	RMSE	nRMSE (%)	*D*	EF	ME	rME (%)
Calibration set									
I	2	880	2391	1512	171.8	0.23	−58.51	1511	171.6
II	7	1070	1138	139	12.9	0.82	0.45	68	6.3
III	7	1829	1691	536	29.3	0.83	0.61	−138	−7.6
IV	4	1597	1413	248	15.5	0.92	0.70	−184	−11.5
V	10	1102	1152	223	20.3	0.95	0.85	49	4.5
Validation set									
VII–IX	12	1740	1827	323	18.6	0.91	0.71	87	5.0

Abbreviations: No.: number of measured/simulated data pairs; X_{obs}: mean of measured yields (kg ha^{-1}); X_{sim}: mean of simulated yields (kg ha^{-1}); RMSE: root mean square error between simulated and measured yields (kg ha^{-1}); nRMSE: normalized RMSE; *d*: index of agreement; EF: model simulation efficiency; ME: mean error (kg ha^{-1}); and rME: relative ME.

the growth pattern of winter lentil, but the seed yields were less well reproduced (Figures S2 and S3). To simulate winter lentil better, knowledge related to low temperature effects on vernalization, dormancy, photosynthesis, N-fixation, and plant (population) survival over winter may be further explored and quantified to improve the model.

4 | CONCLUSIONS

After appropriate parameterizations with data from the literature and various field experiments, the CSM-CROPGRO model simulated well the development and growth of the lentil crop. The performance of the adapted model for lentil appears satisfactory based on comparison of the simulated crop attributes to the observed values. The model generally reproduced well lentil development rate (days to each development stage), LAI, dynamics of biomass accumulation, and seed yield. Graphical comparisons and the statistical evaluations of simulated and observed development and biomass accumulation indicate reasonable performance. Overall, the CSM-CROPGRO-Lentil model appears ready to be applied for simulating lentil development, growth, and production in the DSSAT system.

AUTHOR CONTRIBUTIONS

Qi Jing: Conceptualization; data curation; formal analysis; investigation; methodology; software; writing—original draft. **Kenneth J. Boote**: Conceptualization; data curation; investigation; software; supervision; writing—review and editing. **Kui Liu**: Data curation; writing—review and editing. **Gerrit Hoogenboom**: Software; writing—review and editing. **Jeffrey W. White**: Writing—review and editing. **Ward Smith**: Writing—review and editing. **Guillaume Jégo**: Writing—review and editing. **Brian Grant**: Writing—review

and editing. **Marianne Crépeau**: Writing—review and editing. **Jiali Shang**: Writing—review and editing. **Jiangui Liu**: Methodology; writing—review and editing. **Aston Chipanshi**: Writing—review and editing. **Budong Qian**: Conceptualization; data curation; funding acquisition; methodology; project administration; writing—review and editing.

ACKNOWLEDGMENTS

This study was partly supported by Agriculture and Agri-Food Canada Project J-002303: "Sustainable crop production in Canada under climate change" under the Interdepartmental Research Initiative in Agriculture and Project J-003082: "Assessing diversified crop rotations for reducing GHG emissions, increasing resilience, and adapting to climate change." The authors are indebted to many colleagues who helped them in identifying field experimental data for modeling lentils. These colleagues include, but are not limited to, Drs. Taras Lychuk, Mervin St. Luce, Bill May, and Hakibu Tanko of Agriculture and Agri-Food Canada, Drs. Yvonne Lawley and Cristen MacMillan of the University of Manitoba, and Drs. Sabine Banniza and Kirstin Bett of the University of Saskatchewan.

CONFLICT OF INTEREST STATEMENT

The authors declare no conflicts of interest.

ORCID

Qi Jing https://orcid.org/0000-0001-8707-1861
Kenneth J. Boote https://orcid.org/0000-0002-1358-5496
Gerrit Hoogenboom https://orcid.org/0000-0002-1555-0537
Guillaume Jégo https://orcid.org/0000-0003-0068-234X
Marianne Crépeau https://orcid.org/0000-0002-7254-4483

REFERENCES

Allen, R. G., Pereira, L. S., Raes, D., & Smith, M. (1998). *Crop evapotranspiration: Guidelines for computing crop water requirements* (FAO Irrigation and Drainage Paper 56). FAO.

Baber, K., Jones, C., McPhee, K., Miller, P. R., & Lamb, P. (2023). Nitrogen fixation among pea and lentil varieties in the Northern Great Plains. *Agronomy Journal*, *115*, 2325–2338. https://doi.org/10.1002/agj2.21419

Barker, B. (2023). *Lentil market classes*. Saskatchewan Pulse Growers. https://saskpulse.com/resources/lentil-market-classes/

Bhatty, R. S. (1988). Composition and quality of lentil (*Lens culinaris* Medik): A review. *Canadian Institute of Food Science and Technology Journal*, *21*, 144–160. https://doi.org/10.1016/S0315-5463(88)70770-1

Boote, K. J., Hartwell Allen, J. L., Prasad, P. V. V., & Jones, J. W. (2010). Testing effects of climate change in crop models. In D. Hillel & C. Rosenzweig (Eds.), *Handbook of climate change and agroecosystems* (pp. 109–129). Imperial College Press.

Boote, K. J., Hoogenboom, G., Jones, J. W., & Ingram, K. T. (2009). Modeling nitrogen fixation and its relationship to nitrogen uptake in the CROPGRO model. In T. Bruulsema, L. Ma, & L. R. Ahuja (Eds.), *Quantifying and understanding plant nitrogen uptake for systems modeling* (pp. 13–46). CRC Press, Taylor & Francis Group LLC.

Boote, K. J., Jones, J. W., Hoogenboom, G., & Pickering, N. B. (1998). The CROPGRO model for grain legumes. In G. Tsuji, G. Hoogenboom, & P. Thornton (Eds.), *Understanding options for agricultural production* (pp. 99–128). Springer.

Boote, K. J., Mínguez, M. I., & Sau, F. (2002). Adapting the CROPGRO legume model to simulate growth of faba bean. *Agronomy Journal*, *94*, 743–756. https://doi.org/10.2134/agronj2002.7430

Boote, K. J., & Pickering, N. B. (1994). Modeling photosynthesis of row crop canopies. *HortScience*, *29*, 1423–1434. https://doi.org/10.21273/HORTSCI.29.12.1423

Boote, K. J., Sau, F., Hoogenboom, G., & Jones, J. W. (2008). Experience with water balance, evapotranspiration, and predictions of water stress effects in the CROPGRO model. In L. R. Ahuja, V. R. Reddy, S. A., Saseendran, & Q. Yu (Eds.), *Response of crops to limited water: Understanding and modeling water stress effects on plant growth processes* (pp. 59–103). ASA, CSSA, SSSA. https://doi.org/10.2134/advagricsystmodel1.c3

Boote, K. J., Seepaul, R., Mulvaney, M. J., Hagan, A. K., Bashyal, M., George, S., Small, I., & Wright, D. L. (2021). Adapting the CROPGRO model to simulate growth and production of *Brassica carinata*, a bio-fuel crop. *GCB Bioenergy*, *13*, 1134–1148. https://doi.org/10.1111/gcbb.12838

Chahota, R. K., Sharma, T. R., & Sharma, S. K. (2019). Conventional genetic manipulations. In M. Singh (Ed.), *Lentils* (pp. 43–55). Academic Press.

Erskine, W., Muehlbauer, F. J., & Short, R. W. (1990). Stages of development in lentil. *Experimental Agriculture*, *26*, 297–302. https://doi.org/10.1017/S0014479700018457

FAOSTAT. (2024). *Crops and livestock products*. FAOSTAT. https://www.fao.org/faostat/en/#data/QCL

Farquhar, G. D., & von Caemmerer, S. (1982). Modelling of photosynthetic response to environmental conditions. In O. L. Lange, P. S. Nobel, C. B. Osmond, & H. Ziegler (Eds.), *Physiological plant ecology II: Water relations and carbon assimilation* (pp. 549–587). Springer Berlin Heidelberg.

Gan, Y., Campbell, C. A., Liu, L., Basnyat, P., & McDonald, C. L. (2009). Water use and distribution profile under pulse and oilseed crops in semiarid northern high latitude areas. *Agricultural Water Management*, *96*, 337–348. https://doi.org/10.1016/j.agwat.2008.08.012

Gan, Y., Hamel, C., Kutcher, H. R., & Poppy, L. (2017). Lentil enhances agroecosystem productivity with increased residual soil water and nitrogen. *Renewable Agriculture and Food Systems*, *32*, 319–330. https://doi.org/10.1017/S1742170516000223

Gan, Y., Hanson, K. G., Zentner, R. P., Selles, F., & McDonald, C. L. (2005). Response of lentil to microbial inoculation and low rates of fertilization in the semiarid Canadian prairies. *Canadian Journal of Plant Science*, *85*, 847–855. https://doi.org/10.4141/P04-111

Ghanem, M. E., Marrou, H., Biradar, C., & Sinclair, T. R. (2015). Production potential of lentil (*Lens culinaris* Medik.) in East Africa. *Agricultural Systems*, *137*, 24–38. https://doi.org/10.1016/j.agsy.2015.03.005

Hanlan, T. G., Ball, R. A., & Vandenberg, A. (2006). Canopy growth and biomass partitioning to yield in short-season lentil. *Canadian*

Journal of Plant Science, *86*, 109–119. https://doi.org/10.4141/P05-029

Hoogenboom, G., Jones, J. W., & Boote, K. J. (1992). Modeling growth, development, and yield of grain legumes using Soygro, Pnutgro, and Beangro: A review. *Transactions of the ASAE*, *35*, 2043–2056. https://doi.org/10.13031/2013.28833

Hoogenboom, G., Porter, C. H., Boote, K. J., Shelia, V., Wilkens, P. W., Singh, U., White, J. W., Asseng, S., Lizaso, J. I., Moreno, L. P., Pavan, W., Ogoshi, R. M., Hunt, L. A., Tsuji, G. Y., Jones, J. W., & Usda-Ars, U. (2019). The DSSAT crop modeling ecosystem. In K. J. Boote (Ed.), *Advances in crop modeling for a sustainable agriculture* (pp. 173–216). Burleigh Dodds Science Publishing.

Hoogenboom, G., Porter, C. H., Shelia, V., Boote, K. J., Singh, U., Pavan, W., Oliveira, F. A. A., Moreno-Cadena, L. P., Ferreira, T. B., White, J. W., Lizaso, J. I., Pequeno, D. N. L., Kimball, B. A., Alderman, P. D., Thorp, K. R., Cuadra, S. V., Vianna, M. S., Villalobos, F. J., Batchelor, W. D., … Jones, J. W. (2023). *Decision support system for agrotechnology transfer (DSSAT) version 4.8.2*. DSSAT Foundation. www.DSSAT.net

Jing, Q., Shang, J., Qian, B., Hoogenboom, G., Huffman, T., Liu, J., Ma, B.-L., Geng, X., Jiao, X., Kovacs, J., & Walters, D. (2016). Evaluation of the CSM-CROPGRO-canola model for simulating canola growth and yield at West Nipissing in eastern Canada. *Agronomy Journal*, *108*, 575–584. https://doi.org/10.2134/agronj2015.0401

Jones, J. W., Hoogenboom, G., Porter, C. H., Boote, K. J., Batchelor, W. D., Hunt, L. A., Wilkens, P. W., Singh, U., Gijsman, A. J., & Ritchie, J. T. (2003). The DSSAT cropping system model. *European Journal of Agronomy*, *18*, 235–265. https://doi.org/10.1016/S1161-0301(02)00107-7

Lake, L., & Sadras, V. O. (2021). Lentil yield and crop growth rate are coupled under stress but uncoupled under favourable conditions. *European Journal of Agronomy*, *126*, 126266. https://doi.org/10.1016/j.eja.2021.126266

Liu, K., Bandara, M., Hamel, C., Knight, J. D., & Gan, Y. (2020). Intensifying crop rotations with pulse crops enhances system productivity and soil organic carbon in semi-arid environments. *Field Crops Research*, *248*, 107657. https://doi.org/10.1016/j.fcr.2019.107657

Liu, L., Gan, Y., Bueckert, R., & Van Rees, K. (2011). Rooting systems of oilseed and pulse crops. II: Vertical distribution patterns across the soil profile. *Field Crops Research*, *122*, 248–255. https://doi.org/10.1016/j.fcr.2011.04.003

Martin, T. N., Fipke, G. M., Winck, J. E. M., & Marchese, J. A. (2020). ImageJ software as an alternative method for estimating leaf area in oats. *Acta Agronómica*, *69*, 162–169. https://doi.org/10.15446/acag.v69n3.69401

McKenzie, B. A., & Hill, G. D. (1989). Environmental control of lentil (*Lens culinaris* Medik.) crop development. *The Journal of Agricultural Science*, *113*, 67–72. https://doi.org/10.1017/S0021859600084628

Poggio, L., de Sousa, L. M., Batjes, N. H., Heuvelink, G. B. M., Kempen, B., Ribeiro, E., & Rossiter, D. (2021). SoilGrids 2.0: Producing soil information for the globe with quantified spatial uncertainty. *Soilless*, *7*, 217–240. https://doi.org/10.5194/soil-7-217-2021

Priestley, C. H. B., & Taylor, R. J. (1972). On the assessment of surface heat flux and evaporation using large-scale parameters. *Monthly Weather Review*, *100*, 81–92. https://doi.org/10.1175/1520-0493(1972)100⟨0081:OTAOSH⟩2.3.CO;2

Qian, B., Jing, Q., Zhang, X., Shang, J., Liu, J., Wan, H., Dong, T., & De Jong, R. (2019). Adapting estimation methods of daily solar radiation for crop modelling applications in Canada. *Canadian Journal of Soil Science*, *99*, 533–547. https://doi.org/10.1139/cjss-2019-0018

Rhioui, W., Al Figuigui, J., Boutagayout, A., Zouhar, M., & Belmalha, S. (2023). Effects of organic and inorganic mulching, nettle extract, and manual weeding on weed management under direct-seeded lentil in Meknes region, Morocco. *Crop Protection*, *173*, 106376. https://doi.org/10.1016/j.cropro.2023.106376

Roberts, E. H., Summerfield, R. J., Ellis, R. H., & Stewart, K. A. (1988). Photothermal time for flowering in lentils (*Lens culinaris* Medik.) and the analysis of potential vernalization responses. *Annals of Botany*, *61*, 29–39. https://doi.org/10.1093/oxfordjournals.aob.a087525

Sehgal, A., Sita, K., Kumar, J., Kumar, S., Singh, S., Siddique, K. H. M., & Nayyar, H. (2017). Effects of drought, heat and their interaction on the growth, yield and photosynthetic function of lentil (*Lens culinaris* Medikus) genotypes varying in heat and drought sensitivity. *Frontiers in Plant Science*, *8*, 1776. https://doi.org/10.3389/fpls.2017.01776

Soil Landscapes of Canada Working Group. (2010). Soil landscapes of Canada v3.2. Agriculture and Agri-Food Canada (digital map and database at 1:1 million scale) Soil Landscapes of Canada Working Group. http://sis.agr.gc.ca/cansis

Summerfield, R. J., & Muehlbauer, F. J. (1981). Controlled environments as an adjunct to field research on lentils (*Lens culinaris* Medik.) I. Perspectives, tenets and objectives. *Experimental Agriculture*, *17*, 363–372. https://doi.org/10.1017/S0014479700011819

Summerfield, R. J., Muehlbauer, F. J., & Roberts, E. H. (1984). Controlled environments as an adjunct to field research on lentils (*Lens culinaris* Medik.). III. Photoperiodic lighting and consequences for flowering. *Experimental Agriculture*, *20*, 1–18. https://doi.org/10.1017/S0014479700017543

Summerfield, R. J., Muehlbauer, F. J., & Short, R. W. (1989a). Controlled environments as an adjunct to field research on lentils (*Lens culinaris* Medik.). V. Cultivar responses to above- and below-average temperatures during the reproductive period. *Experimental Agriculture*, *25*, 327–341. https://doi.org/10.1017/S0014479700014848

Summerfield, R. J., Muehlbauer, F. J., & Short, R. W. (1989b). Controlled environments as an adjunct to field research on lentils (*Lens culinaris* Medik.). IV. Cultivar responses to above- and below-average temperatures during vegetative growth. *Experimental Agriculture*, *25*, 119–134. https://doi.org/10.1017/S0014479700016501

Summerfield, R. J., Roberts, E. H., Erskine, W., & Ellis, R. H. (1985). Effects of temperature and photoperiod on flowering in lentils (*Lens culinaris* Medik.). *Annals of Botany*, *56*, 659–671. https://doi.org/10.1093/oxfordjournals.aob.a087055

Van Kessel, C. (1994). Seasonal accumulation and partitioning of nitrogen by lentil. *Plant and Soil*, *164*, 69–76. https://doi.org/10.1007/BF00010112

Wang, F. (2017). SIOX plugin in ImageJ: Area measurement made easy. *UV4Plants Bulletin*, *2016*, 37–44. https://doi.org/10.19232/uv4pb.2016.2.11

Whitehead, S. J., Summerfield, R. J., Muehlbauer, F. J., Coyne, C. J., Ellis, R. H., & Wheeler, T. R. (2000). Crop improvement and the accumulation and partitioning of biomass and nitrogen in lentil. *Crop Science*, *40*, 110–120. https://doi.org/10.2135/cropsci2000.401110x

Wright, D. M., Neupane, S., Heidecker, T., Haile, T. A., Chan, C., Coyne, C. J., McGee, R. J., Udupa, S., Henkrar, F., Barilli, E., Rubiales, D., Gioia, T., Logozzo, G., Marzario, S., Mehra, R., Sarker, A., Dhakal, R., Anwar, B., Sarkar, D., … Bett, K. E. (2021). Understanding photothermal interactions will help expand production range and increase

genetic diversity of lentil (*Lens culinaris* Medik.). *Plants People Planet*, *3*, 171–181. https://doi.org/10.1002/ppp3.10158

Zakeri, H., Bueckert, R. A., Schoenau, J. J., Vandenberg, A., & Lafond, G. P. (2012). Controlling indeterminacy in short season lentil by cultivar choice and nitrogen management. *Field Crops Research*, *131*, 1–8. https://doi.org/10.1016/j.fcr.2012.02.027

Zakeri, H., Lafond, G. P., Schoenau, J. J., Pahlavani, M. H., Vandenberg, A., May, W. E., Holzapfel, C. B., & Bueckert, R. A. (2012). Lentil performance in response to weather, no-till duration, and nitrogen in Saskatchewan. *Agronomy Journal*, *104*, 1501–1509. https://doi.org/10.2134/agronj2011.0339

Zakeri, H., Schoenau, J., Vandenberg, A., Tayfeh Aligodarz, M., & Bueckert, R. A. (2015). Indirect estimations of lentil leaf and plant N by SPAD chlorophyll meter. *International Journal of Agronomy*, *2015*, 748074. https://doi.org/10.1155/2015/748074

SUPPORTING INFORMATION

Additional supporting information can be found online in the Supporting Information section at the end of this article.

How to cite this article: Jing, Q., Boote, K. J., Liu, K., Hoogenboom, G., White, J. W., Smith, W., Jégo, G., Grant, B., Crépeau, M., Shang, J., Liu, J., Chipanshi, A., & Qian, B. (2024). Simulating the development and growth of lentil using the CSM-CROPGRO model. *Agronomy Journal*, *116*, 2391–2410. https://doi.org/10.1002/agj2.21654